

HiSST: 4th International Conference on High-Speed Vehicle Science Technology 22 -26 September 2025, Tours, France



Effects of Temperature and Thermal Aging on the Microstructure and Mechanical Behavior of C/C-SiC Ultra-High Temperature Ceramic Matrix Composites

Nicholas D. Parolini¹, Abhendra K. Singh²

Abstract

In hypersonic flights, hot structural materials capable of maintaining structural integrity at high temperatures are needed for various vehicle components. In response to this, interest has grown in ultra-high temperature ceramic matrix composites (UHTCMCs). The work performed in this investigation looks at the changes in microstructure and mechanical strength of short-term thermal exposure and thermal aging of C/C-SiC UHTCMC. The studies are performed at 600°C and 1200°C. After being thermally exposed, all samples showed a loss in mass. Closer inspection of the thermally exposed C/C-SiC samples showed erosion in the fibers, matrix, as well as the fiber and matrix interface. EDS scans detected oxygen co-located in carbon rich areas of the composites, indicating that there was a preferential oxidation of carbon in the thermally exposed samples. Disk compression tests of the samples indicated that the splitting tensile strength of the composites decreases with increasing time and temperature of exposure. Differences in failure modes were also observed due to differences in temperature and duration of exposure.

Keywords: C/C-SiC, UHTCMCs, CMCs, Refractory Composites, Hypersonics

1. Introduction

Hot structures in hypersonic and atmospheric re-entry vehicles demand materials capable of withstanding extreme environments without compromising the structural integrity [1-4]. Historically, ceramic matrix composites (CMCs) and other refractory composites such as carbon/carbon (C/C) have been used for external hot structures in these applications due to their high strength to weight ratios, thermal stability, and mechanical performance [1-3, 5]. However, with the push toward reaching higher velocities, the resulting thermal loading exceeds the capabilities of current material systems. In response to this challenge, interest has grown in ultra-high temperature ceramics (UHTCs), which are capable of withstanding high temperatures in excess of 2000°C [2-6]. However, they are often limited by their low fracture toughness and thermal shock resistance [2-4]. To address this, a new material class that combines the fracture toughness and thermal shock resistance of CMCs with the high temperature capabilities of UHTCs, known as ultra-high temperature ceramic matrix composites (UHTCMCs), is increasingly gaining prominence [4]. Notable examples of these materials include Carbon/Zirconium Diboride (C/ZrB₂), Carbon/Carbon-Zirconium carbide (C/C-ZrC), and Carbon/Hafnium Diboride(C/HfB₂) [2, 3, 5].

While not strictly classified as a UHTCMC, Carbon/Carbon-Silicon Carbide (C/C-SiC) is often grouped with UHTCMCs due to its proven operational use at temperatures up to 2000°C for short durations and under vacuum conditions [7-10]. C/C-SiC composites offer improved oxidation resistance from C/C

¹ Baylor University Department of Mechanical Engineering, Waco, TX, USA, 76704, <u>nick_parolini1@baylor.edu</u>

² Baylor University Department of Mechanical Engineering, Waco, TX, USA, 76704, <u>abhen_singh@baylor.edu</u>

HiSST-2025-337

Page | 1

composites. Also, they are able to to operate for longer durations at temperatures up to 1700°C, have high strength to weight ratio, and good thermal shock resistance [2, 4, 9, 11]. This makes it an attractive candidate for hypersonic and reusable space flight applications.

One of the key limitations of UHTCMCs, such as those incorporating C and SiC, is oxidation [2, 3, 5]. Historically, carbon-based constituents in refractory composites, i.e. carbon fibers and matrix, begin to oxidize at temperatures as low as 500°C in air, leading to the formation of gaseous byproducts of either CO or CO₂ [11-14]. As this reaction occurs, pits and voids will form in both the matrix and fibers of the composite [11, 13, 14]. In the fibers particularly, oxidation will cause changes in the overall morphology of the fiber, i.e., sharp fiber ends and pitting in the fibers [15, 16]. Silicon carbide is also subject to oxidation with increasing temperatures in air and can begin at temperatures as low as 600°C through either an active or passive oxidation reaction [17-21]. In active oxidation, SiC will react with oxygen creating volatile SiO and CO gaseous products, and often occurs when the supply of oxygen is too low and at temperatures below 1200°C [20, 21]. The passive oxidation of SiC will form a protective SiO₂ layer and CO gas, and occurs at temperatures at or above 1200°C [18-21].

Given the present interest in C/C-SiC UHTCMC, understanding the effects of extreme temperature environments on the composition, microstructure, and mechanical properties of these composites is critical for advancing these next generation material systems for use in hot structures. This study investigates the effects of short-term exposure and thermal aging on the microstructure and mechanical behavior of C/C-SiC UHTCMCs. Short term exposure tests were conducted to simulate the effects of a short-duration flight (<20minutes) and thermal aging was performed to evaluate the long-term exposure effects. The overarching goal of this study is to compare the effectiveness of C/C-SiC UHTCMCs in short and long term extreme thermal environmental conditions.

2. Material and Test Methodology

2.1. Material and Test Specimen Fabrication

The C/C-SiC used in this study was manufactured and provided by Exothermics, Inc., NH, USA. The parent plate was fabricated through the assembly of unidirectional tape plies stacked in a $[\pm 45/0/90]_{15}$ layup. Two types of specimens were manufactured from this parent plate. These were disk specimens, which were used for mechanical evaluation through disk-compression testing, and Cuboid or "control" specimens, which were exposed alongside the disk specimens and used to compare microstructural changes in the specimens due to thermal exposure. Fig. 1 shows a diagram of how both specimen geometries are cut from provided parent plate material. The disk specimens were cut using a 12.7mm diamond coated tile coring drill and were 8.4 ± 0.3 mm in diameter. They were further sliced to a thickness of 2.35 ± 0.46 mm using a diamond coated bandsaw. Control specimens were also cut using a diamond coated band saw and had a nominal size of 8.5 mm x 8.0 mm x 14.5 mm. All cutting and drilling operations performed in the fabrication of the specimens using a water-based coolant to keep the specimens from overheating, and avoid excessive cutting damage, i.e. broken fibers and matrix debris, on the surface of the composite.

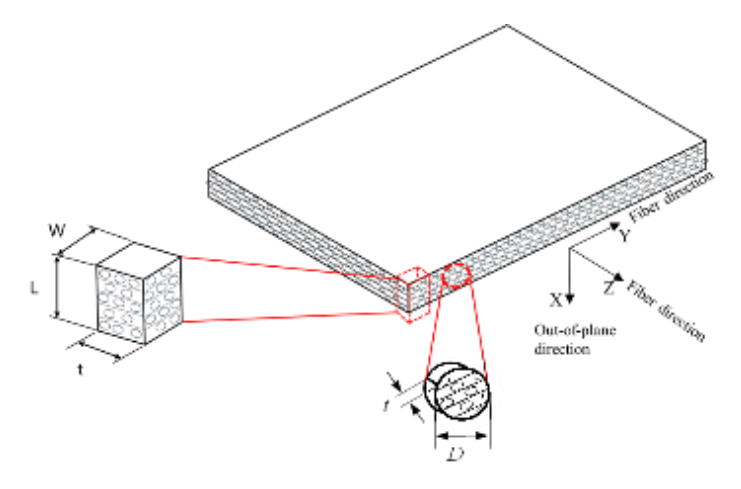


Fig 1. Diagram showing where disk and control specimens were cut from the parent material.

2.2. Thermal Exposure and Mechanical Evaluation

Short-term and long-term thermal exposure studies were conducted on both disk and control specimens to evaluate the effects of oxidation on the sample. Thermal exposure was carried out at two key temperatures in air, 600°C and 1200°C. The temperature of 600°C corresponds to the onset of SiC oxidation, and exceeds the oxidation onset temperature for carbon in the composite [11, 14, 17-21]. The 1200°C test condition was chosen as it corresponds to the active to passive oxidation transition temperature of SiC [11, 14, 17-21].

Short term thermal exposure mechanical tests, denoted ET600 and ET1200 were performed at 600° C and 1200° C, respectively. The mechanical tests were performed by the disk-compression method using a compact AMTECO air-based furnace at both temperatures. Results were compared to disk-compression tests performed at room temperature. The test set-ups for both the pristine and elevated temperature tests are presented in Fig. 2. In both cases, alumina ceramic rods were used to load the specimens. For the mechanical tests at elevated temperature, the disks were placed inside the furnace and furnace was ramped from ambient conditions to 204° C at a rate of 120° C/min. It was then held isothermally for 30 minutes at 204° C to evaporate any moisture trapped within the furnace. The furnace was further ramped to the target temperature at 120° C/min, and held isothermally for 20 minutes before the mechanical test was performed. The 20-minute hold simulated the exposure times consistent with short duration flight profiles [22]. Control samples were placed in the furnace chamber in the elevated temperature tests, which were solely dedicated to microstructural evaluations. For the control samples, masses were measured before and after exposure using a Mettler Toledo scale with a ± 0.002 -gram tolerance.

Three disk-compression tests were performed at room temperature and three each at each elevated temperature condition. The tests were performed using an Instron 3382A electromechanical load frame, with a crosshead displacement of 0.5 mm/min and a 100 kN load frame. Strain measurement in both test set ups was performed using an Aramis, GOM 2D digital image correlation system (DIC) equipped with blue light sources. Room-temperature and thermally aged specimens were speckled using commercially available black and white Rustoleum paints, whereas, elevated temperature test specimens were speckled using Aremco pyro-paint alumina and SiC based paints [23]. A blue band pass filter was added to the DIC camera in elevated temperature testing to block undesirable light wavelengths as well as maintain light consistency in testing. All DIC measurements were recorded at a rate of 7 frames per second. To mitigate the optical distortion that can come because of heat haze in the elevated temperature tests, extra alumina fabric insulation was placed around the openings in the furnace, and a fan was directed at the space between the camera and the furnace viewport to stabilize the airflow around the camera.

Long term thermal exposure, or thermal aging, studies were performed to understand the effects of prolonged high temperature exposure on the material. Thermal aging was conducted using a SentroTech high temperature furnace at 600° C and 1200° C, denoted TA600 and TA1200 respectively. The furnace was ramped at a rate of 3° C/min until the target temperature, at which point the specimens were held isothermally for 30 hours to simulate a cumulative lifetime exposure of the space shuttle, corresponding to a design life of 100 missions with a flight to and from orbit of 8.5 minutes [24]. For the thermally aged samples, masses were measured before and after exposure using a Mettler Toledo scale with a ± 0.002 -gram tolerance. Some of the thermally aged samples were used for microstructure evaluations while three samples per condition were used for disk-compression mechanical tests at room temperature, as discussed subsequently.

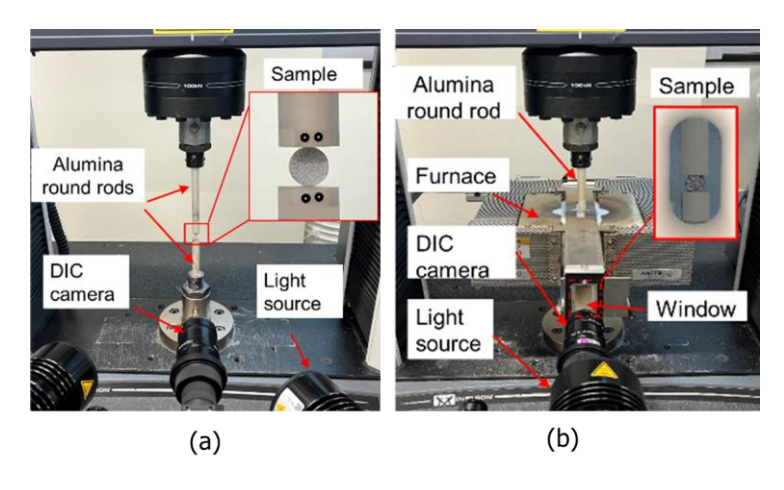


Fig 2. Images showing the (a) the mechanical testing set up at room temperature, and (b) the mechanical testing set up for short term thermal exposure testing.

2.3. Microstructural and Compositional Evaluation

Microstructural and compositional changes resulting from thermal exposure were evaluated using x-ray diffraction (XRD), scanning electron microscopy (SEM), optical microscopy, and energy dispersive spectroscopy (EDS). XRD scans were conducted using a Siemens D-5000 diffractometer using a step size of 0.02° at a rate of 1 second per step rotating from 10 to 90° . The detected material peaks in the C/C-SiC composite were identified according to published values in literature on Bragg's angle [21, 26, 27]. SEM was conducted using both a Versa 3D and a Jeol SEM, the latter equipped with an EDS system. Prior to evaluation, control samples were sectioned using a QATM precision cut off saw with a diamond coated cut off wheel. Each sectioned sample was used for microstructural evaluation. Half of the sample was used for surface morphology studies and microstructural imaging via SEM, and optical microscopy using a Keyence VHX-7000 optical microscope. The other half was mounted in epoxy resin with the internal region of the composite facing out for imaging and was polished for use with SEM. Polishing started with grinding the samples flat with a 240-grit sandpaper followed by 400-grit and 600-grit sandpaper polishing. This was immediately followed with a diamond slurry polish using 9 µm, 3 µm, and 1 µm slurries, while washing samples in an ultrasonic bath in between each polishing step.

Thermogravimetric analysis (TGA) was conducted to evaluate the thermal stability and oxidizing behaviors of C/C-SiC. Sliver specimens of the composite were prepared for TGA using a diamond coated band saw to create samples that initially weighed between 20 and 40 mg. TGA was performed using a TA Discovery Series 550 system capable of reaching temperatures up to 1000°C in both air and nitrogen environments. Two test protocols were used. The first protocol heated the specimen from room temperature to 1000°C in air to observe key inflection points in the temperatures where rapid changes in weight would occur. The second looked at weight losses at 600°C. This test heated the specimen in nitrogen until 600°C, then switched the atmosphere in the TGA to air, allowing the sample to oxidize for 100 minutes. Both tests were run using a heating rate of 15°C/min from room temperature until 300°C, then followed by a final ramp to the desired temperature at a rate of 3°C/min. A high temperature platinum pan was used to hold the samples in the TGA in all tests.

3. Results and Discussion

3.1. Physical and Microstructural Changes

Observation of C/C-SiC after thermal exposure showed some effects of oxidation on the mass and color of the specimens. When comparing the masses of the samples before and after exposure, the thermally exposed specimens showed weight losses depending on the temperature intensity and exposure duration in testing. Fig. 3a shows the average change in the masses of the disks before and after thermal exposure. Mass losses were observed to be in excess of 35% for the thermally aged and

ET1200 specimens. However, in the ET600 case, the observed mass losses were less than 5%. TGA revealed that as the specimens were heated in air until 1000°C, there was an observed increase in the rate of weight loss between 600°C and 950°C as shown in Fig. 3b. Starting at 600°C, the change in weight with respect to temperature increases to a rate of 0.1%/°C while in air. When held isothermally in air at 600°C, the specimens held a linear weight loss rate of 0.1%/°C as shown in Fig. 3c.

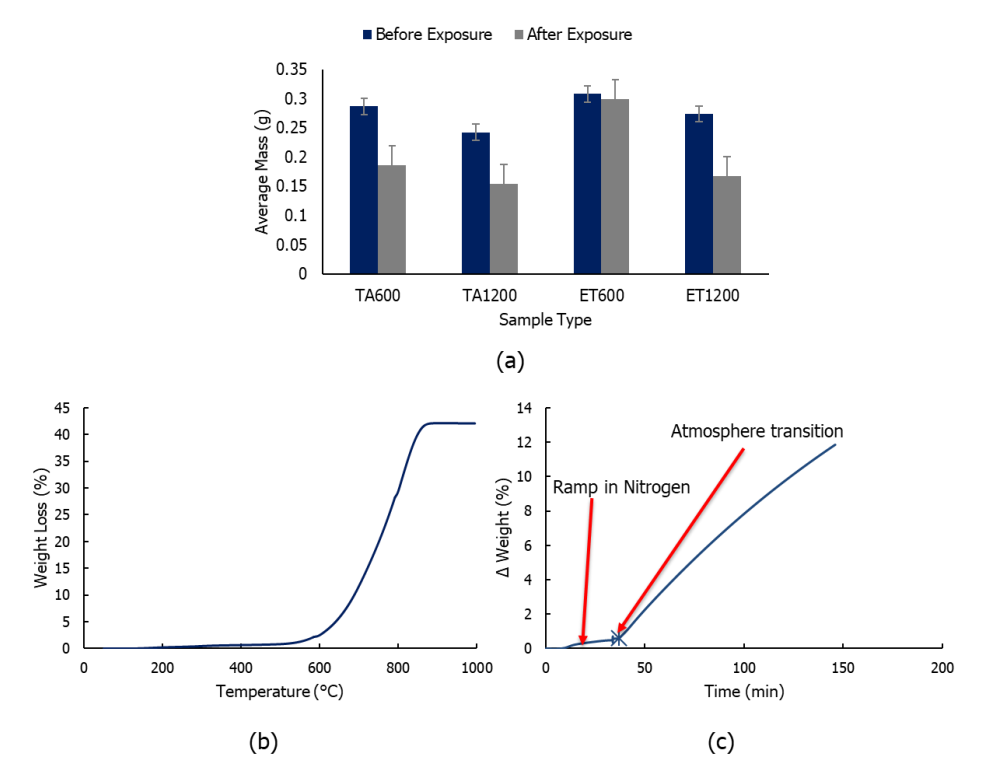


Fig 3. Graphs showing the changes in mass (a) relative to the sample exposure duration and temperature of exposure (b) when samples are ramped in air to 1000° C, and (c) held isothermally at 600° C.

After thermal exposure there was a change in color for each of the thermally exposed specimens, with some notable oxide scale formation in the TA1200 specimens. This change in color is consistent with previous studies in which both carbon in the fibers and the matrix would change color as the specimens began to oxidize [15, 16]. Looking at the cross sections of the thermally exposed control samples shown in Fig. 4, the color of the specimens change to a varying degree in each case depending on the time and temperature of thermal exposure. The TA600 and ET1200 cases in Fig. 4 show that only a portion of the material has changed color going through the thickness of the material. Compared to these cases, the TA1200 case shows a color change throughout the thickness of the material due to the time and temperature of exposure. However, when looking at the ET600 case, the cross-section appears similar to the pristine case where there is minimal change in color through the thickness of the specimen, and that color change due to oxidation was only surface level on the specimen.

Further inspection of the surface and cross sections of the C/C-SiC samples reveal microstructural changes with thermal exposure. Fig. 5 shows the surface and cross-sectional SEM micrographs for each thermally exposed case. In the pristine specimen cases, the fibers are well consolidated physically to the carbon and SiC constituents in the matrix. As oxygen diffuses through the material, this consolidation or adherence degrades. Micrographs of the thermally aged cases show that as the C/C-SiC oxidizes, the carbon fibers and matrix erode on the surface. This results in the disappearance of fibers from the surface of the composite, leaving behind residual matrix films or "fiber shells" on the surface of the composites as well as matrix voids. Additionally, cross-sectional micrographs of the TA1200 case revealed the presences of fiber bundles coated in SiO₂. When looking at the ET600 and ET1200 results in Fig. 5, the ET1200 surface micrographs show similar results to the thermally aged cases. Upon closer inspection of the surface morphology in the ET600 case, matrix erosion is observed on the surface, leaving behind matrix voids and standing fibers. In the cross-sectional micrographs for

each thermal exposure, case, there is an observed degradation in the fiber-matrix interface, as well as some fiber degradation that occurs as a result of oxidation.

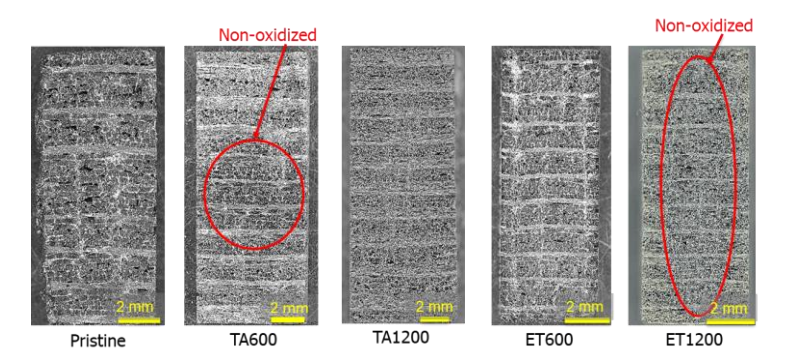


Fig 4. Cross-Sectional optical microscope images of the exposed control samples showing varying degrees of oxygen diffusion with the time and temperature of thermal exposure.

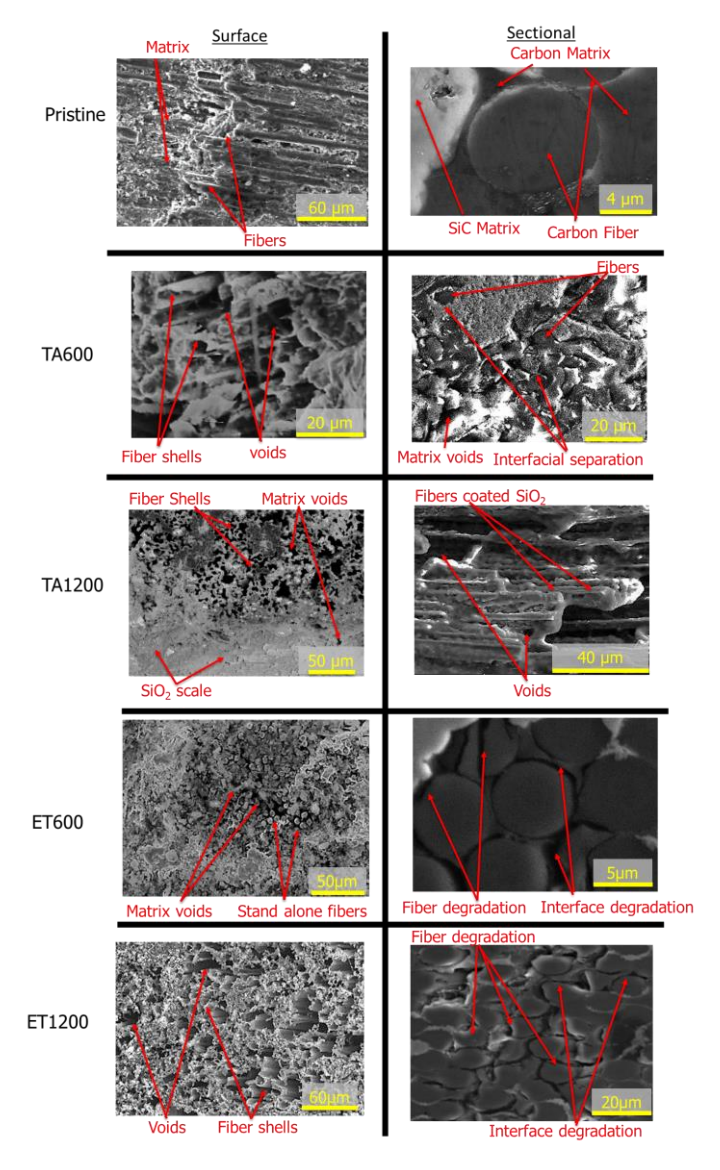


Fig 5. Surface and cross-sectional SEM micrographs for each thermal exposure case.

EDS mapping was used to characterize the chemical compositional changes of C/C-SiC with thermal exposure. The presence of oxygen was detected in each of the thermally exposed cases and appears co-located in carbon rich regions of the composite in larger concentrations. As exposure time increases, there is an observable increase in the amount of oxygen present in the samples. This measured between 12-19% in the TA1200 samples in comparison to 4-5% in the ET1200 samples. Higher magnification analysis of the fibers (Fig. 6) further reveals that the oxidation affects the fiber-matrix interfacial region in much larger concentrations than the fibers or matrix separately.

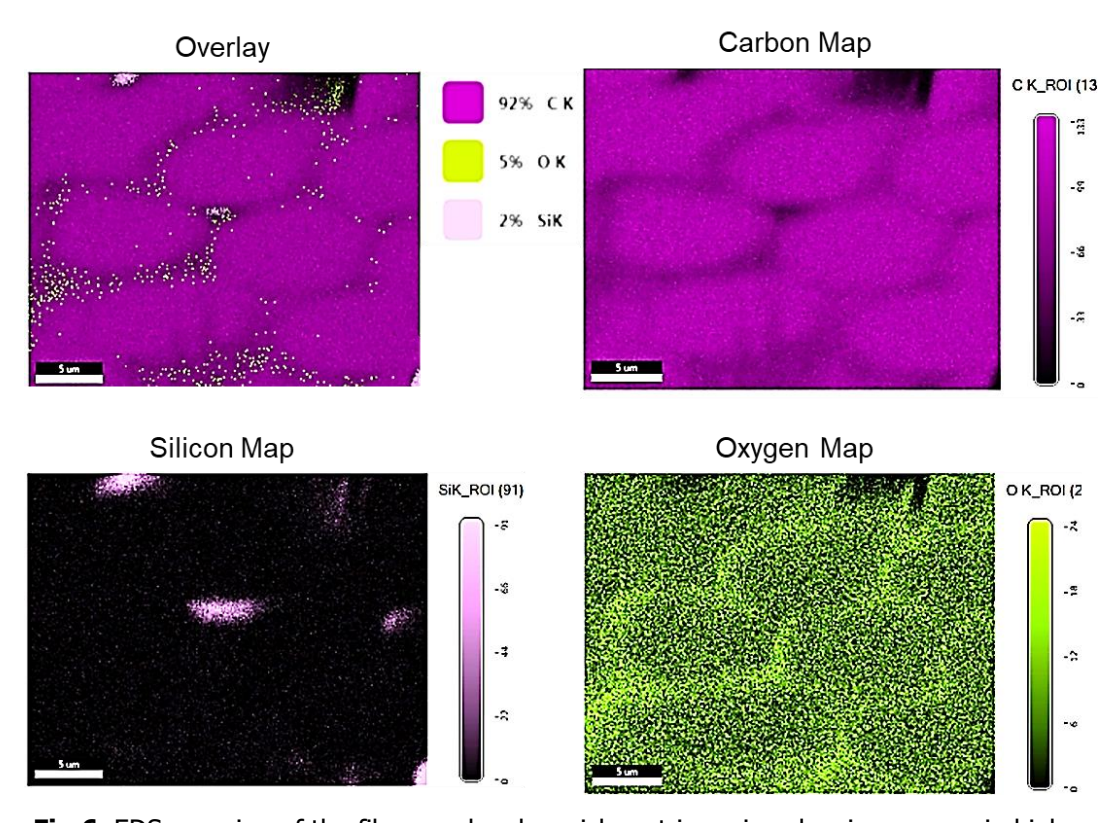


Fig 6. EDS mapping of the fibers and carbon rich matrix region showing oxygen in higher concentrations around the fiber-matrix interface.

As the C/C-SiC specimens were subjected to thermal exposure, there were also changes in the material phase composition as revealed by XRD. Fig. 7 shows the XRD plots for each of the different thermal exposure conditions observed. In all the thermally exposed cases, there is a reduction of surface level carbon, even in the ET600 case, indicating there is a preferential oxidation of carbon over SiC in the specimens. In the thermally aged specimens, there are observed decreases in the detected free silicon and SiC in both cases. In the TA1200 case in particular, there is an observed increase in the detection of SiO₂, indicating that passive oxidation is occurring resulting in the formation of oxide scales on the surface of the material. When considering the ET600 and ET1200 cases, there is an increase in the detection of free silicon in the specimens as the carbon oxidizes from the surface of the specimens. Additionally, in the ET1200 case, there is a slight increase in the peaks corresponding to SiO₂ [21, 25, 26].

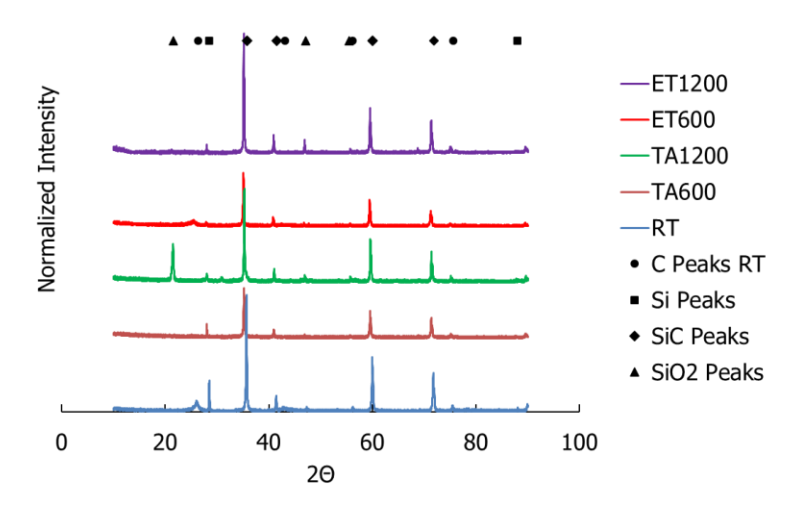


Figure 7. XRD normalized intensity plots and identified constituent peaks.

3.2. Mechanical Strength Evaluation

The splitting tensile strength was calculated using Equation 1 [24-32]:

$$S = \frac{2P}{\pi Dt} \tag{1}$$

where S is the splitting tensile strength of the disk, P is the applied compressive load, D is the diameter of the disk, and t is the thickness. Equation 1 allows for a simplified means of comparing the mechanical strengths of the disks but relies on several assumptions: linear elastic behavior, material isotropy and homogeneity, symmetric and uniform loading behavior, and plane stress conditions throughout the disk [24, 26, 28-32]. Some of these are not true for the material being investigated in this study. Therefore, this equation is used just as a means of comparing mechanical performance and does not assert to be evaluating the interlaminar tensile strength of the composite.

The disk-compression test allowed for a direct comparison between the fracture behaviors of C/C-SiC after thermal aging (long term exposure) and at direct elevated temperature testing (short term exposure). All results were compared to tests performed in pristine samples at room temperature. Fig. 8 shows the splitting tensile strengths of each of the thermally exposed conditions, and Table 1 shows the average strengths at each thermal exposure condition, as well as how they compare to the pristine case. The splitting tensile strengths of C/C-SiC appear to diminish with prolonged thermal exposure for both 600°C and 1200°C. Compared to the pristine room temperature strengths, the TA600 and TA1200 cases show that after 30 hours of exposure, there is a decrease in the splitting tensile strengths by 71-82%.

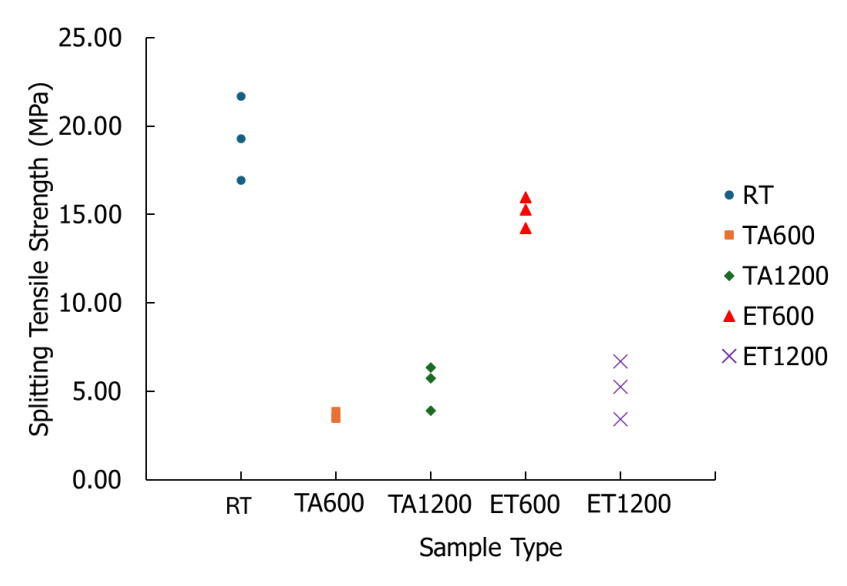


Fig 8. Splitting tensile strengths evaluated for each thermal exposure condition.

Table 1. Average splitting tensile strengths from each thermally exposed condition and their comparisons to the pristine condition.

Condition	Average Splitting Tensile Strength	Percent Difference from RT (%)
RT	19.5	NA
TA600	3.6	81
TA1200	5.3	72
ET600	15.2	22
ET1200	5.1	73

After short durations of exposure, the splitting tensile strengths of C/C-SiC show an overall decrease. As Table 1 shows, after 20 minutes of exposure at 600°C, there is a decrease in the splitting tensile strength of 22%, compared to the ET1200 and thermally aged cases which see strength losses in excess of 70%. However, when considering the ET1200 case, the decrease in strength is on the same order of the thermally aged response, indicating that there is a rapid decrease in strength that happens at 1200°C regardless of the time of exposure.

The failure modes between the different thermal exposure cases showed different behaviors depending on the time and temperature of exposure. Fig. 9a shows the representative load displacement curves from each thermal exposure case. For the pristine and ET600 cases, the specimens show an approximately linear loading response until a singular load drop where a catastrophic failure occurs in the disk. This load drop indicates the formation of a singular crack down the line of loading of the specimen, indicating a transversal tensile failure. Fig. 9b shows a representative DIC image of the splitting failure observed in the room temperature and ET600 test conditions. In comparison to the pristine and ET600 cases, the ET1200 and thermally aged cases showed different failure modes, consisting of a mixture of both crushing and splitting failures. Fig. 9c shows representative catastrophic failure of the disk for the ET1200, and thermally aged cases. As the load displacement curves in Fig. 9a show, these specimens showed a non-linear load response with multiple load drops corresponding

to localized crushing behaviors at the loading points of the disks, followed by a final drop in the load corresponding to a split in the disk.

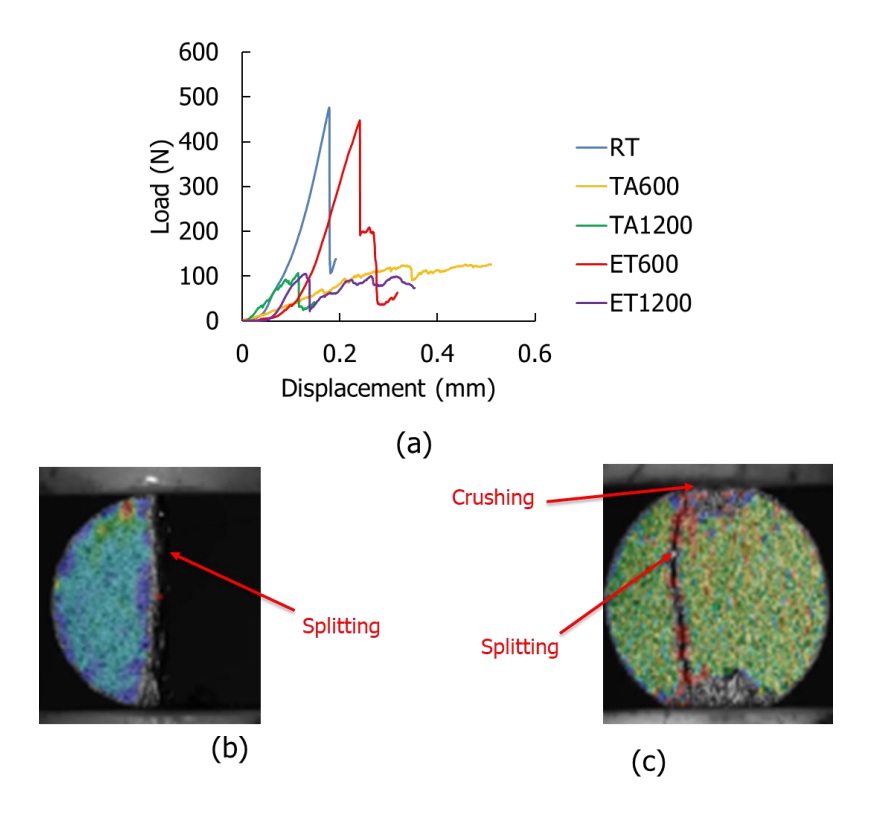


Fig 9. Representative (a) load-displacement curves for each thermally exposed case, (b) failures in the RT and ET600 thermally exposed cases, and (c) failure modes observed in the thermally aged and ET1200 cases.

Further characterization of the failure mechanisms using SEM and optical microscopy corroborated the observations made by DIC. Representative fractography results of the pristine and ET600 cases is shown in Fig. 10a, while Fig. 10b shows the representative fractography results of the ET1200 and thermally aged cases. In the pristine and ET600 cases, cracks formed through the compressive loading of the disk specimens transversed the matrix rich interlaminar and fiber dominated intralaminar regions of the specimen. In contrast, the ET1200 and thermally aged cases exhibited additional damage features, including evidence of broken and fractured fibers and the existence of matrix voids and fiber shells. Localized crushing deformations were also observed near the loading regions of the ET1200 and thermally aged cases.

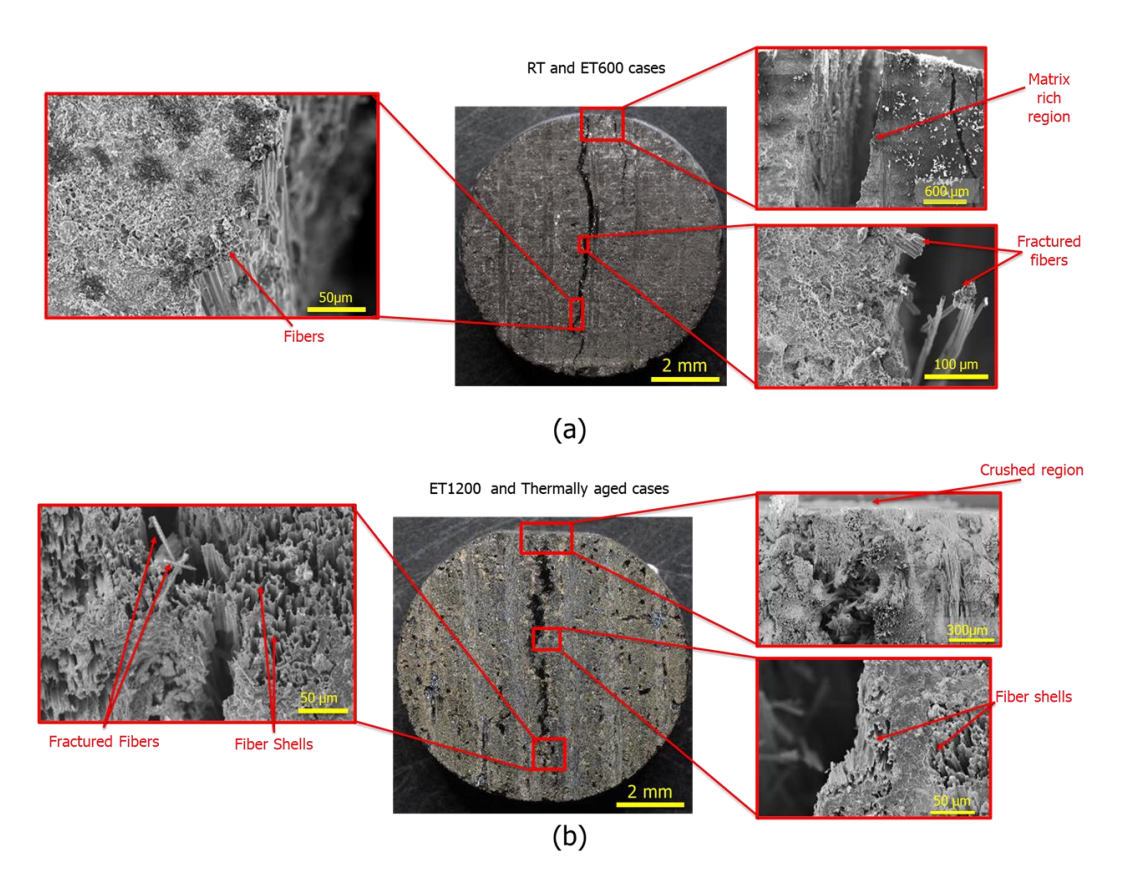


Fig 10. Representative failure modes for (a) the RT and ET600 cases, and (b) the ET1200, and thermally aged cases.

4. Summary and Conclusions

Hot structures in hypersonic and space flight vehicles demand material systems capable of maintaining structural integrity under prolonged durations of high temperature exposure. In this study C/C-SiC UHTCMCs were evaluated for their thermo-structural integrity after high temperature exposures for varying time durations. Thermal aging was performed at 600°C and 1200°C for 30 hours on both disk and control specimens as well as short duration exposure at the same temperatures for 20 minutes. Evidence of oxidation was observed in all cases, manifested through a measurable mass loss in the specimens depending on the time and temperature of exposure, and discoloration of the carbon fibers and matrix in the material. SEM observations revealed the presence of fiber and matrix erosion in the sample. EDS detected oxygen co-located in carbon rich areas of the thermally exposed composites, and in larger concentrations around the fiber-matrix interfacial regions of the composite.

Mechanical testing demonstrated that the degree of strength reduction was strongly dependent on the time and temperature of thermal exposure. Disk-compression testing showed that reductions in splitting tensile strength in excess of 72% for both the thermally aged cases and for short duration exposure at 1200°C. For the short duration 600°C case, reduction in strength was 22%. Furthermore, failure modes were observed to change from a splitting failure in the pristine and short exposure case at 600°C to a mixed splitting and crushing failure in the short exposure 1200°C and thermally aged cases. These preliminary results indicate the susceptibility of C/C-SiC UHTCMCs to oxidative degradation under sustained high temperature environments.

5. References

- 1. Glass, D.: Ceramic Matrix Composite (CMC) Thermal Protection Systems (TPS) and Hot Structures for Hypersonic Vehicles. 15th AIAA Conference, Dayton, Ohio. (2008). doi: 10.2514/6.2008-2682.
- 2. Binner, J., Porter, M., Baker, B., Zou, J., Venkatachalam, V., Diaz, V.R., D'Angio, A., Ramanujam, P., Zhang, T., Murthy, T.S.R.C.: Selection, processing, properties and applications of ultra-high temperature ceramic matrix composites, UHTCMCs a review. Int. Mat. Rev., 65, 7, 389–444 (2020). doi: 10.1080/09506608.2019.1652006.
- 3. Rueschhoff, L. M., Carney, C. M., Apostolov, Z. D., Cinibulk, M. K.: Processing of fiber-reinforced ultra-high temperature ceramic composites: A review. IJCES, 2, 1, 22–37 (2020). doi: 10.1002/ces2.10033.
- 4. Zoli, L., Vinci, A., Galizia, P., Melandri, C., Sciti, D.: On the thermal shock resistance and mechanical properties of novel unidirectional UHTCMCs for extreme environments. Sci. Rep., 8, 1, 9148 (2018). doi: 10.1038/s41598-018-27328-x.
- 5. Baier, L., Frieß, M., Hensch, N., Leisner, V.: Development of ultra-high temperature ceramic matrix composites for hypersonic applications via reactive melt infiltration and mechanical testing under high temperature. CEAS Space J (2024). doi: 10.1007/s12567-024-00562-y.
- 6. Ni, D., Cheng, Y., Zhang, J., Liu, J., Zhou, J., Chen, B., Wu, H., Li, H., Dong, S., Han, J., Zhang, X., Fu, Q., Zhang, G.: Advances in ultra-high temperature ceramics, composites, and coatings. J. Adv. Ceram., 11, 1, 1–56 (2022). doi: 10.1007/s40145-021-0550-6.
- 7. Hald, H., Ullmann, T.: Reentry Flight and Ground Testing Experience with Hot Structures of C/C-SiC Material. 44th AIAA/ASME/ASCE/AHS/ASC Structures. (2003). doi: 10.2514/6.2003-1667.
- 8. Heidenreich, B.: Carbon fibre reinforced sic materials based on melt infiltration. 6th International Conference on High Temperature Ceramic Matrix Composites. (2007)
- 9. Singh, J. P., Bansal, N.P. Goto, T., Lamon, J., Choi, S.R., Mahmoud, M. M., Link, G.: Processing and Properties of Advanced Ceramics and Composites IV. John Wiley & Sons (2012)
- 10. Krenkel, W.: Carbon Fibre Reinforced Silicon Carbide Composites (C/SiC, C/C-SiC). Handb. Ceram. Compos. Springer US, Boston. 117–148. (2005). doi: 10.1007/0-387-23986-3 6.
- 11. Jacobson, N. S., Curry, D. M.: Oxidation microstructure studies of reinforced carbon/carbon. Carbon, 44, 7, 1142–1150, (2006). doi: 10.1016/j.carbon.2005.11.013.
- 12. Li, C., Brown, T. C.: Carbon oxidation kinetics from evolved carbon oxide analysis during temperature-programmed oxidation. Carbon, 39, 5, 725–732 (2001). doi: 10.1016/S0008-6223(00)00189-5.
- 13. Guo, W., Xiao, H., Yasuda, E., Cheng, Y.: Oxidation kinetics and mechanisms of a 2D-C/C composite. Carbon, 44, 15, 3269–3276, (2006). doi: 10.1016/j.carbon.2006.06.027.
- 14. Labruquère, S., Bourrat, X., Pailler, R., Naslain, R.: Structure and oxidation of C/C composites: role of the interface. Carbon, 39, 7, 971–984 (2001). doi: 10.1016/S0008-6223(00)00142-1.
- 15. Singh, S., Srivastava, V. K.: Effect of oxidation on elastic modulus of C/C–SiC composites. Mater. Sci. Eng. A, 486, 1, 534–539 (2008). doi: 10.1016/j.msea.2007.09.078.
- 16. Hui, Y., Liu, G., Zhang, Q., Zhang, Y., Zang, Y., Wang, S., Shi, R.: Fading behavior and wear mechanisms of C/C–SiC brake disc during cyclic braking. Wear, 526–527, 204930 (2023). doi: 10.1016/j.wear.2023.204930.
- 17. Naslain, R., Guette, A., Rebillat, F., Le Gallet, S., Lamouroux, F., Filipuzzi, L., Louchet, C.: Oxidation mechanisms and kinetics of SiC-matrix composites and their constituents. J. Mater. Sci., 39, 24, 7303–7316 (2004). doi: 10.1023/B:JMSC.0000048745.18938.d5.
- 18. Jacobson, N. S., Myers, D. L.: Active Oxidation of SiC. Oxid Met, 75, 1, 1–25 (2011). doi: 10.1007/s11085-010-9216-4.

- 19. Jacobson, N. S., Fox, D. S., Opila, E. J.: High temperature oxidation of ceramic matrix composites. Pure Appl. Chem., 70, 2, 493–500, (1998). doi: 10.1351/pac199870020493.
- 20. Jones, R. H.: Environmental effects on engineered materials. Corrosion technology, no. 15. Marcel Decker, New York (2001)
- 21. Nasiri, N. A., Patra, N., Ni, N., Jayaseelan, D. D., Lee, W. E.: Oxidation behaviour of SiC/SiC ceramic matrix composites in air. J. Eur. Ceram. Soc., 36, 14, 3293–3302, (2016). doi: 10.1016/j.jeurceramsoc.2016.05.051.
- 22. "U.S. Hypersonic Weapons and Alternatives | Congressional Budget Office." Accessed: May 26, 2025. Available: https://www.cbo.gov/publication/58924
- 23. Le, V. T., Parolini, N., Shih, C., Singh A. K.: Interlaminar tensile strength of Alumina-Based Oxide/Oxide ceramic matrix composite at room temperature and 1200 °C using diametral compression test method. Composi. Part A Appl. Sci. Manuf., 186, 108420, (2024). doi: 10.1016/j.compositesa.2024.108420.
- 24. "The Space Shuttle NASA." Accessed: Mar. 24, 2025. Available: https://www.nasa.gov/reference/the-space-shuttle/
- 25. Yao, J., Pang, S., Hu, C., Li, J., Tang, S., Cheng, H.-M.: Mechanical, oxidation and ablation properties of C/(C-SiC)CVI-(ZrC-SiC) PIP composites. Corros. Sci., 162, 108200, (2020). doi: 10.1016/j.corsci.2019.108200.
- 26. Zhang, K. X., Guo, X. S., Cheng, Y. X., Zhang, F. Q., He, L. L.: TEM study on the morphology and interface microstructure of C/C-SiC composites fabricated by liquid infiltration. Mater. Charact., 175, 111055, (2021). doi: 10.1016/j.matchar.2021.111055.
- 27. Choi, Y. B., Hinoki, T., Ozawa, K., Katoh, Y., Matsugi, K., Kelimu, T.: Strength Anisotropy of NITE-SiC/SiC Composite by Various Failure Modes. Mater. Trans., 53, 11, 2060–2063, (2012). doi: 10.2320/matertrans.M2012182.
- 28. Mattison, J. T., Faucett, D. C., Choi, S. R.: Development of High-Temperature, Interlaminar Tension Test Methodology for Ceramic Matrix Composites. J. Eng. Gas Turbines Power, 147, 011008, (2024). doi: 10.1115/1.4066288.
- 29. Newton, C. D., Jeffs, S. P., Gale, L., Pattison, S., Bache, M. R.: Determining the interlaminar tensile strength of a SiCf/SiC ceramic matrix composite through diametrical compression testing. J. Eur. Ceram. Soc., 43, 7, 2951–2957, (2023). doi: 10.1016/j.jeurceramsoc.2022.11.014.
- 30. Es-Saheb, M. H., Albedah, A., Benyahia, F.: Diametral compression test: validation using finite element analysis. Int. J. Adv. Manuf. Technol., 57, 5–8, 501–509, (2011). doi: 10.1007/s00170-011-3328-0.
- 31. Timoshenko, S., Goodier, J. N.: Theory of Elasticity. McGraw-Hill (1969)
- 32. Faisal, N. H., Mann, L., Duncan, C., Dunbar, E., Claton, M., Frost, M., McConnachie, J., Fardan, A., Ahmed, R.: Diametral compression test method to analyse relative surface stresses in thermally sprayed coated and uncoated circular disc specimens. Surf. Coat. Technol., 357, 497–514, (2019). doi: 10.1016/j.surfcoat.2018.10.053.